Tracer dispersion in 2-D fractures with flat and rough walls in a radial flow geometry

I. Ippolito
Laboratoire de Physique et Mécanique des Milieux Hétérogènes (URA-CNRS No. 857), ESPCI, 10 rue Vauquelin, 75231 Paris Cedex 05, France

E. J. Hinch
Department of Applied Mathematics and Theoretical Physics, Cambridge University, Cambridge CB3 9EW, England

G. Daccord
Dowell Schlumberger, ZI de Molina la Chazotte, BP90, 42003 Saint-Etienne Cedex 1, France

J. P. Hulin
Laboratoire de Physique et Mécanique des Milieux Hétérogènes (URA-CNRS No. 857), ESPCI, 10 rue Vauquelin, 75231 Paris Cedex 05, France

(Received 17 February 1993; accepted 28 April 1993)

Tracer dispersion is studied in a plane fracture geometry with a radial flow between closely spaced parallel walls with either two smooth surfaces or one smooth and one rough surface. An echo dispersion technique in which the fluid is first injected into the fracture during a time T_{inv} and then pumped back through a detector is used in the experiments and is complemented by Monte-Carlo-type numerical simulations. For the smooth wall case, the Taylor dispersion mechanism is dominant when longitudinal molecular diffusion is negligible: it is verified numerically and experimentally that its transition to irreversibility only depends on the ratio of T_{inv} to the transverse diffusion time τ_m across the fracture thickness. In addition, the variation of $\overline{\Delta T^2}/(4T_{\text{inv}}\tau_m)$ with respect to T_{inv}/τ_m is the same as for a flow of parallel geometry ($\overline{\Delta T^2}$ being the mean square deviation of the transit time). Longitudinal molecular diffusion increases the global dispersion like $T_{\text{inv}}/(\text{Pe}_Q\tau_m)$ at low Péclet numbers Pe_Q and long times due to the longitudinal velocity gradient. When one of the walls is rough, one expects to have a geometrical dispersion locally proportional to the velocity. A corresponding linear variation of $\overline{\Delta T^2}/(4T_{\text{inv}}\tau_m)$ with respect to $\sqrt{T_{\text{inv}}/\text{Pe}_Q}$ is observed experimentally.

I. INTRODUCTION

Transport of fluid or chemical species in fractured rocks is a topic of widespread interest because of its numerous practical applications in areas such as petroleum, nuclear, chemical, and environmental engineering or hydrogeology.[1] From the point of view of the geometrical and velocity field structures, fractured media represent an excellent example of heterogeneous materials: effectively, they very often display a broad range of characteristic length scales and their transport properties are strongly dependent on the connectivity and the spatial distribution of the flow channels. For instance, in a system of fractures with a very broad distribution of apertures, the effective flow paths may involve only a small fraction of all fractures building up a sublattice of continuous paths made of the largest fractures.[2,3] For individual fractures, the roughness of the fracture walls may strongly influence the structure of the flow inside them and the relation between their mean aperture and the individual permeability of each fracture.[4]

It is therefore very important to characterize these flow field heterogeneities both at the scale of an individual fracture and at that of a system of many fractures. The present paper concentrates on the first problem: It presents an experimental study of single model fractures with a well-defined geometry and both smooth and rough walls in a radial flow field.

Tracer dispersion has been chosen as our experimental tool since it is very sensitive to flow heterogeneities and spatial velocity variations. It corresponds to the spreading of an initially localized tracer concentration distribution carried along by a flowing fluid through the medium of interest. Tracer dispersion is induced by the combined effects of molecular diffusion, velocity gradients inside individual flow channels and velocity variations from one channel to another;[5,6] its use in fractured media has already been suggested by other authors.[7]

More specifically, we have used an echo dispersion measurement[8,9] where tracer is first injected into the system during a controlled time T_{inv} and then pumped back through a detector (Fig. 1). This technique is better adapted to radial flow than transmission dispersion in which tracer moves all the way through the sample toward an outlet detector; it also can give complementary information. Transmission dispersion is very sensitive to macroscopic length and velocity variations on the flow paths between the injection and detection points. On the contrary, we shall see that echo dispersion is mostly sensitive to local structure parameters such as the fracture mean aperture or its roughness. In addition, echo dispersion allows one to study the influence of the time lapse T_{inv} between the initial injection of tracer into the sample and the reversal of the flow; T_{inv} is proportional to the mean depth

 0899-8213/93/5(8)/1952/11/$6.00

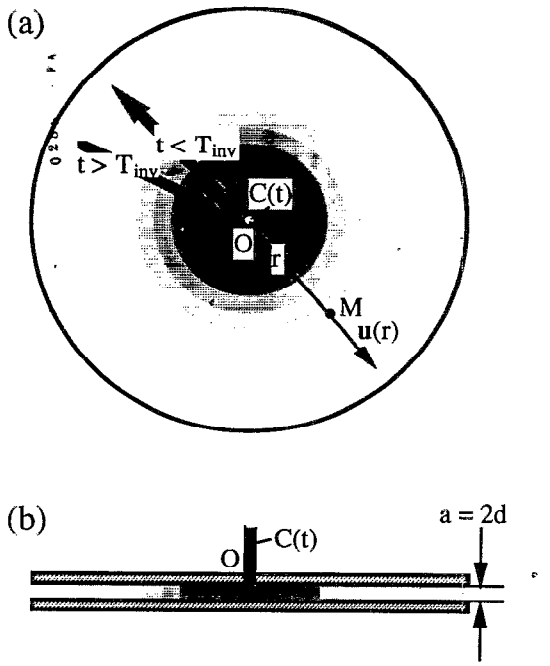

FIG. 1. Principle of an echo dispersion experiment in the radial Hele–Shaw cell flow geometry. An invading solution (dark shading) is injected locally during a time T_{inv} to displace a solution of different tracer concentration (light shading) initially saturating the cell. It is then pumped back through a detector measuring the variation $C(t)$ of the tracer concentration. (a) View from above; (b) side view.

of penetration of the tracer into the sample.

We have also chosen to study the case of radial flow field (Fig. 1) which is a good approximation to the flow that would be induced by a local injection of fluid performed for instance inside a well or a borehole. It is not possible to obtain simple analytical solutions for the advection–diffusion equation in radial flow for the general case in which all dispersion mechanisms need to be taken into account: This is due to the dependence of the dispersion coefficient on velocity which varies with distance.

We shall first present the Taylor dispersion mechanism[10,11] which is always present in two-dimensional (2-D) planar flow geometries. We shall then consider qualitatively how this basic mechanism is modified in a radial geometry in which the flow velocity decreases with distance from the injection point. In particular, we shall show that molecular diffusion is dominant both at very short and very long times, while Taylor dispersion is more important in the intermediate range. Our hypothesis will be confirmed by numerical simulations which establish the dependence of the boundary between the various dispersion regimes on the flow velocity and on the geometrical parameters of the fracture. Then, we shall compare these theoretical results to those of experiments performed on a model structure made of two parallel glass plates. Finally we shall analyze the influence of the roughness of the fracture walls by comparing experimental results obtained with a model fracture with rough walls to the previous ones. The geometry is then closer to that of fractures in a real rock. We shall show that, in this case, geometrical dispersion associated with the flow field disorder may be dominant at low velocities as it is in many three-dimensional (3-D) porous media.

II. QUALITATIVE ANALYSIS OF ECHO TRACER DISPERSION IN A RADIAL FLOW FIELD INSIDE A 2-D FRACTURE

A. Gaussian tracer dispersion

In homogeneous systems, the variation of the tracer concentration C satisfies the classical advection–diffusion equation:[6]

$$\frac{\partial C}{\partial t}+U\frac{\partial C}{\partial x}=D_{\parallel}\frac{\partial^2 C}{\partial x^2}+D_{\perp}\left(\frac{\partial^2 C}{\partial y^2}+\frac{\partial^2 C}{\partial z^2}\right), \tag{1}$$

where U is the constant mean tracer velocity, and $D_{\parallel}$ and $D_{\perp}$ characterize, respectively, longitudinal (x direction) and transverse (y and z) dispersion relative to the mean flow direction. Equation (1) describes a "Gaussian" or normal dispersion for one-dimensional (1-D) flow. It is only valid if the dispersion process is the combination of a large number of uncorrelated steps[12,13] (a similar hypothesis is stated in the central limit theorem). This assumption is not valid when large size flow inhomogeneities are present.

Generally, $D_{\parallel}$ is larger than the molecular diffusion coefficient D_m. Both are of the same order of magnitude only at very low flow velocities. The relative magnitude of the convective and diffusive effects is characterized by means of the Péclet number $\mathrm{Pe}=Ud/D_m$ (d is the characteristic aperture of the flow channels). Molecular diffusion is dominant when Pe is typically lower than 10.

B. Taylor dispersion mechanism

The first dispersion mechanism we study is Taylor dispersion:[10] it is associated with the local velocity gradients in the Poiseuille velocity profile between the center of the channel and the walls. Taylor dispersion is usually studied in capillary tubes, although it will also be present in the flow between two plane parallel walls representing the simplest type of fracture. In a tube with a circular section, the longitudinal Taylor dispersion coefficient $D_{\parallel}$ varies as the square of the mean velocity for high enough Péclet number values:[11]

$$D_{\parallel}=\frac{R^2U^2}{48D_m}+D_m, \tag{2}$$

where R is the radius of the capillary and the last term in Eq. (2) corresponds to pure molecular diffusion.

Let us consider qualitatively the physical mechanism leading to Eq. (2).[14] Let us induce at $t=0$ an abrupt variation of the tracer concentration C at $x=0$. If there were no transverse molecular diffusion, the concentration variation would propagate as a sharp front at the local velocity $u(r)$ given by the parabolic law:

$$u(r)=2U\left(1-\frac{r^2}{R^2}\right) \tag{3}$$

[where $u(r)$ is the velocity at a distance r from the tube axis and U the average velocity across the cross section]. The front would then be spread over a distance Δx increasing linearly with time:

$$\Delta x_{\text{conv}}=2Ut. \tag{4}$$

Molecular diffusion, however, acts radially to homogenize the concentration over the cross section and so limits the development of the parabolic profile. Let us define the characteristic molecular diffusion time τ_m of the tracer particles across the section of the tube as $\tau_m=R^2/D_m$. Around this time τ_m, there is a transition toward a diffusive spreading regime where the front thickness Δx increases as

$$\Delta x_{\text{diff}}\propto\sqrt{D_{\parallel}\,t}. \tag{5}$$

At the transition time $t=\tau_m$, one has $\Delta x_{\text{conv}}\simeq\Delta x_{\text{diff}}$ so that $D_{\parallel}\propto U^2R^2/D_m$ in agreement with the high-velocity limit of the rigorous equation (2).

In the plane fracture geometry which is of interest to us, similar results are obtained. For a parallel constant velocity flow field between two parallel flat plates with smooth surfaces, the dispersion coefficient at long times becomes[11]

$$D_{\parallel}=\frac{a^2U^2}{210D_m}+D_m, \tag{6}$$

where a is the distance between the plates.

C. Echo Taylor dispersion in radial and parallel flows

Let us see now how these results are modified in the echo process that has been used in our experiments. In this technique, one first allows the tracer to penetrate into the flow channel before reversing the flow at time $t=T_{\text{inv}}$ and monitoring then the returning concentration variation in the injection plane $x=0$. In laminar flows, the local velocity $u_x(r)$ at all points in the flow tube becomes $-u_x(r)$ when the global flow direction is reversed. Therefore, in the absence of molecular diffusion, the linear spreading Δx_{conv} given by Eq. (4) would be reversed and all particles would return to the plane $x=0$ at time $t=2T_{\text{inv}}$. This reversibility is approached at small inversion times $T_{\text{inv}}\ll\tau_m$ when longitudinal molecular diffusion is expected to be the dominant spreading mechanism. At long times $T_{\text{inv}}\gg\tau_m$, the tracer concentration will be more homogenized across the flow and the tracer particles will lose all the "memory" of their initial transverse position. Then, the effective dispersion is expected to be identical to that obtained in a transmission experiment with the same total duration $2T_{\text{inv}}$. This argument is applicable to both the parallel plane and the circular tube geometries.

Let us now consider the influence on the tracer dispersion of the velocity gradients present in the radial geometry used in the present paper. Fluid flows radially with a flow rate Q from an injection point O between two infinite plane walls separated by a distance $a=2d$. Let the Oz axis be perpendicular to the solid walls located at $z=\pm d$. The radial velocity field is

$$u(r,z)=\frac{3Q}{8\pi dr}\left(1-\frac{z^2}{d^2}\right) \tag{7a}$$

so that the mean velocity $U(r)$ averaged over the spacing between the plates is

$$U(r)=Q/4\pi\,dr. \tag{7b}$$

Therefore, the velocity decreases with r and, at sufficiently large distances, the local Péclet number $\text{Pe}=U(r)2d/D_m$ becomes low enough for molecular diffusion to be the dominant spreading factor.

1. Echo Taylor dispersion for Pe≫1

In this case, we assume that molecular diffusion *parallel* to the flow is always negligible compared to hydrodynamic Taylor-like dispersion. Let us compare the two geometries of a uniform flow parallel to the direction x and of a radial flow. In the parallel flow, the distance x traveled by a tracer particle after the time T_{inv} is given by

$$x=U\int_0^{T_{\text{inv}}}\left(1-\frac{z(t)^2}{d^2}\right)dt$$

where the coordinate $z(t)$ is a random variable representing the molecular diffusion of the tracer particles between the two plates. At time T_{inv}, the velocity U becomes $-U$ and the particle reaches again the plane $x=0$ after a time t such that

$$U\int_0^{T_{\text{inv}}}\left(1-\frac{z(t)^2}{d^2}\right)dt-U\int_{T_{\text{inv}}}^{t}\left(1-\frac{z(t)^2}{d^2}\right)dt=0. \tag{8}$$

The dispersion in the values of t reflects only the changes of the return times from one realization of the random variable $z(t)$ to another. For a radial flow, the distance r of the particle from the injection point satisfies Eq. (7a):

$$\frac{dr}{dt}=\frac{3Q}{8\pi\,dr}\left(1-\frac{z^2}{d^2}\right),$$

whence, by straightforward integration,

$$r^2(t)-r_0^2=\frac{3Q}{4\pi d}\int_0^{T_{\text{inv}}}\left(1-\frac{z(t)^2}{d^2}\right)dt.$$

A comparison of this result with Eq. (8) leads to the important conclusion that the tracer particle returns to the circle of radius r_0, from where it started, at a time t given by exactly the same equation as for parallel flow. This result is not surprising since the transition from the parallel to the radial flow case is only a matter of change of variables. Therefore the transit time distributions for echo experiments performed in these two flow geometries are identical and controlled by the only parameters T_{inv}, d, and D_m. More precisely, as remarked above qualitatively, it is the ratio of the inversion time T_{inv} and the characteristic transverse diffusion time $\tau_m=d^2/D_m$ (across the channel half-width d) that determines the degree of reversibility of the dispersion (this point will be discussed in more detail below).

At times large compared to τ_m the Taylor dispersion process will be completely irreversible. If the local Péclet number is still large in radial flow, the width of the transit time distribution is the same as for a transmission dispersion experiment with the same total duration $\bar{T}=2T_{\text{inv}}$ in parallel flow. The effective dispersion coefficient is therefore given by Eq. (6) where the D_m term is neglected:[15]

$$D_{\parallel}=\frac{U^2}{2}\frac{\overline{\Delta t^2}}{\bar{T}}=\frac{U^2(2d)^2}{210D_m} \tag{9a}$$

or

$$\frac{\overline{\Delta t^2}}{4T_{\text{inv}}}=\frac{2d^2}{105D_m}, \tag{9b}$$

where $\overline{\Delta t^2}$ is the mean square deviation of the transit time of the tracer particles. At lower inversion times T_{inv} (but still when Pe$\gg$1), Eq. (9) will be replaced, according to the previous discussion by the following relation:

$$\frac{\overline{\Delta t^2}}{4T_{\text{inv}}\tau_m}=g\left(\frac{T_{\text{inv}}}{\tau_m}\right)\frac{2}{105}, \tag{10}$$

where the function $g(x)$ tends toward 1 at large x and describes the approach of the dispersion process to irreversibility.

2. Transition to irreversibility for echo Taylor dispersion (Pe$\gg$1, $T_{inv}<\tau_m$)

Let us now consider qualitatively the variation of $\overline{\Delta t^2}$ with T_{inv} where $g(T_{\text{inv}}/\tau_m)$ is lower than 1. Let us assume that the local Péclet number $U(r)d/D_m$ is always $\gg$1. We shall use the simple case of a parallel Poiseuille flow of velocity $u(z)$ between two parallel planes since we have shown that the transition to irreversibility is the same as in the radial case. Consider a particle initially at $x=0$ and $z=z_0$ when $t=0$. The particle is convected parallel to Ox at the local velocity $u[z(t)]$ and makes in addition a sideways random Brownian motion $\delta z(t)$ with a variance $\overline{\delta z^2(t)} \sim D_m t$. At short times $t\ll\tau_m$, the mean lateral distance $\sqrt{\overline{\delta z^2(t)}}$ explored is much smaller than the distance d between the planes. One can therefore assume that the variations of the longitudinal velocity experienced by the particles correspond to a constant local shear rate $\gamma(z_0)=(\partial u/\partial z)(z_0)$. These longitudinal velocity variations result in a deviation $\delta x(z_0,t)$ with respect to the mean displacement $x_0(z_0,t)=u(z_0)t$:

$$\delta x(z_0,t)\sim\gamma(z_0)\int_0^t \delta z(t')dt'. \tag{11}$$

Thus the order of magnitude of the mean square deviation of the longitudinal displacement of the particles with respect to the mean value $x_0(z_0,t)$ will be

$$\overline{\delta x^2(z_0,t)}\sim\gamma^2(z_0)\overline{\delta z^2(z_0,t)}t^2\sim\gamma^2(z_0)D_m t^3. \tag{12}$$

This deviation $\overline{\delta x^2(z_0,t)}$ corresponds to irreversible dispersion. This is the only mechanism present in echo experiments when $T_{\text{inv}}<\tau_m$ since the spreading associated with the dependence of $u(z_0)$ on z_0 is reversible and does not contribute to echo dispersion. Now, the displacement $\delta x(z_0,t)$ is related to the deviation $\delta t(z_0)$ in the transit times along a path by $\delta x(t)=u(z_0)\delta t(z_0)$. So,

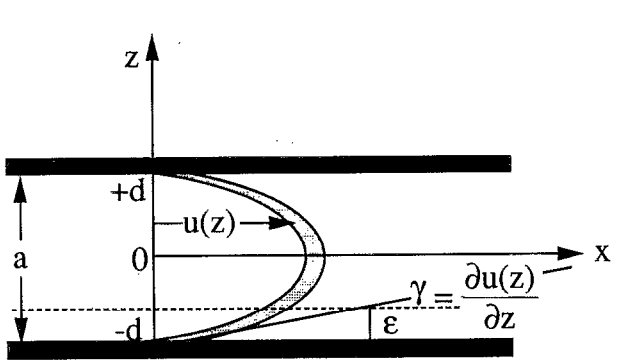

FIG. 2. Poiseuille flow velocity $u(z)$ between two parallel flat plates with a shear rate $\gamma=\partial u(z)/\partial z$ at the walls for $T_{\text{inv}}<\tau_m$. $\Delta z=\sqrt{D_m t}$ represents the order of magnitude of the distance of the wall over which tracer spreads through molecular diffusion during the time t.

$$\overline{\delta t^2(z_0)}\sim D_m t^3\frac{\gamma^2(z_0)}{u^2(z_0)}. \tag{13}$$

The global echo dispersion results from an average over all particles launched at various z_0. We therefore average $\overline{\delta t^2(z_0)}$ by integrating over all the possible values of z_0. The dominant contribution clearly comes from the low-velocity part of the flow (Fig. 2). There is a problem near the walls where the integral diverges: we shall take the range of integration to stop within the distance $\sqrt{D_m t}$ of the walls where the particles can diffuse during the transit time t. If we assume that particles are released from $x=0$ at $t=0$ with a uniform distribution of z values between $-d$ and $+d$, one obtains

$$\overline{\Delta t^2}=\langle\overline{\delta t^2(z)}\rangle\sim\frac{1}{2d}\int_{-d+\sqrt{D_m t}}^{d-\sqrt{D_m t}}\overline{\delta t^2}(z)\,dz. \tag{14}$$

Substituting expression (13) we obtain

$$\overline{\Delta t^2}\sim\frac{1}{d}\int_0^{d-\sqrt{D_m t}} D_m t^3\frac{\gamma^2(z)}{u^2(z)}dz. \tag{15}$$

Near the important top boundary $u(z)\approx\gamma(d-z)$, so

$$\overline{\Delta t^2}\sim\frac{1}{d}D_m t^3\int_0^{d-\sqrt{D_m t}}\frac{1}{(d-z)^2}dz. \tag{16}$$

Integrating expression (16) for $t=2T_{\text{inv}}$ we obtain for $\sqrt{D_m t}\ll d$:

$$\frac{\overline{\Delta t^2}}{T_{\text{inv}}}\sim\frac{\sqrt{D_m}}{a}T_{\text{inv}}^{3/2}. \tag{17}$$

Finally, substituting $\tau_m=a^2/D_m$ one has

$$\frac{\overline{\Delta t^2}}{T_{\text{inv}}\tau_m}\sim\left(\frac{T_{\text{inv}}}{\tau_m}\right)^{3/2}. \tag{18}$$

We see from (18) that the mean square time deviation $\overline{\Delta t^2}/(T_{\text{inv}}\tau_m)$ does not vary with the velocity but only depends on the ratio T_{inv}/τ_m, as assumed in Eq. (10). Note

that the final result of Eq. (18) depends on the way in which the tracer is injected. Instead of spreading the initial tracer concentration uniformly in the range $[-d,+d]$, let us assume that the injection is modulated proportional to the local velocity. In this case, the above analysis yields a variation of $\overline{\Delta t^2}/(T_{\rm inv}\tau_m)$ proportional to $(T_{\rm inv}/\tau_m)^2 \ln(T_{\rm inv}/\tau_m)$ instead of $(T_{\rm inv}/\tau_m)^{3/2}$.

The estimates in this section for $\mathrm{Pe}\gg 1$ and $T_{\rm inv}<\tau_m$ have ignored longitudinal molecular dispersion. At very short injection times, the longitudinal molecular dispersion distance $\sqrt{D_m T_{\rm inv}}$ may theoretically exceed the advection $UT_{\rm inv}$. This happens when $T_{\rm inv}/\tau_m < 1/\mathrm{Pe}^2$. It is not possible practically to perform experiments in this regime so that we will not analyze it further.

3. Radial echo Taylor dispersion at long times when Pe ≲ 1

The above result is only valid when the flow velocity is large enough so that locally $\mathrm{Pe}\gg 1$. At very long injection times in the radial geometry, the velocity can decrease sufficiently as the tracer moves away from the injection point so that the local Péclet number becomes less than unity. Equation (6) is still valid as long as $t\gg\tau_m$ but now, the molecular diffusivity is retained:

$$D[U(r)]=\frac{4d^2U^2(r)}{210D_m}+D_m, \tag{19}$$

where $U(r)$ is the mean velocity given by Eq. (7b). Now, $D_{\|}/U^2$ does depend on the velocity U and, therefore, on the distance r from the injection point and Eq. (9a) must be replaced by the differential equation:

$$D_{\|}(U)=\frac{U^2}{2}\frac{d(\overline{\Delta t^2})}{d\bar{T}}, \tag{20a}$$

so that for an echo experiment with an inversion time $T_{\rm inv}$:

$$\overline{\Delta t^2}=\int_0^{2T_{\rm inv}} 2\frac{D[U(r)]}{U^2(r)}\,dt. \tag{20b}$$

Equations (20a) and (20b) imply that, in order to compute the resultant dispersion from zones corresponding to different velocities, one has to sum the contributions of each zone to $\overline{\Delta t^2}$ and not those to $\overline{\Delta x^2}$. The contribution to $\overline{\Delta t^2}$ from a given zone is indeed unchanged as the velocity varies, while that to $\overline{\Delta x^2}$ decreases as fluid particles crowd together as they slow down. Let us now use Eq. (7b) to estimate the mean time $t(r)$ to reach a radius r away from the injection point ($r=r_0$). One has $r^2=Qt(r)/2\pi d$ if $r_0\ll r$. Let us now combine this latter expression with Eqs. (19), (20b), and (7b), obtaining by integration:

$$\overline{\Delta t^2}(2T_{\rm inv})=\frac{8d^2}{105D_m}T_{\rm inv}+\frac{16\pi d D_m T_{\rm inv}^2}{Q}. \tag{21}$$

Here $\overline{\Delta t^2}(2T_{\rm inv})$ is the mean square width of the transit time distribution of tracer particles during an echo experiment. Replacing d^2/D_m by τ_m, and defining a global Péclet number by $\mathrm{Pe}_Q=2rU(r)/D_m=Q/2\pi dD_m$ which is constant with the distance r, one obtains

$$\frac{\overline{\Delta t^2}(2T_{\rm inv})}{4T_{\rm inv}\tau_m}=\frac{2}{105}+\frac{T_{\rm inv}}{\mathrm{Pe}_Q\tau_m}. \tag{22}$$

The first term in Eq. (22) corresponds to Taylor dispersion and implies that the Taylor regime is reached ($T_{\rm inv}\gg\tau_m$). The second term is the longitudinal molecular diffusion contribution to tracer spreading: it becomes important for low Pe_Q numbers and for large values of either $T_{\rm inv}$ or the penetration distance.

III. NUMERICAL SIMULATION OF TRACER DISPERSION IN A RADIAL FLOW BETWEEN FLAT PARALLEL WALLS

A. Monte Carlo simulations of Taylor dispersion in a radial geometry

In Monte Carlo simulations, tracer particles are assumed to move independently of each other. One follows the radial and vertical displacements of a large number of particles moving in the Hele–Shaw cell. The motion of each particle is the combination of the effects of molecular diffusion (represented by a Brownian motion) and convection by the radial flow field (modulated by the parabolic Poiseuille velocity profile between the plates). Because of the radial symmetry, one can ignore the motion in the angular direction. The random Brownian motion is simulated by changing the radial and the vertical positions separately at each time step by

$$\sqrt{6D_m\Delta t}\times\mathrm{rand}, \tag{23}$$

where D_m is the molecular diffusion coefficient, Δt is the time-step, and rand is a random number chosen uniformly on the interval $[-1,1]$. (Particular care has to been taken to use a random number generator that produces good independent random numbers, as required here for each particle for each time step and for each direction.) The amplitude $\sqrt{6D_m\Delta t}$ of the random steps has been chosen so that the variance of any coordinate after n independent steps is

$$\overline{[x(t)-x(0)]^2}=n6D_m\Delta t\tfrac{1}{3}=2D_m t, \tag{24}$$

where the factor 1/3 represents the variance of a random number chosen uniformly on $[-1,1]$.

The radial flow is incorporated with a radial displacement at each time step:

$$\frac{Q}{4\pi\,dr}\frac{3}{2}\left(1-\frac{z(t)^2}{d^2}\right)\Delta t, \tag{25}$$

where Q is the volume flux and d is the channel half-width. More sophisticated time-stepping procedures are pointless because the random part of the motion produces a velocity which is highly discontinuous and all the sophisticated procedures require highly continuous derivatives. Equation (25) corresponds to the Hele–Shaw approximation[16] for the velocity field between the plates. It will be valid except very near the injection point because of the large ratio between the typical values of r and the half-width d.

Zero flux boundary conditions at the top and bottom of the channel are implemented by reflecting conditions. Thus

if a random step takes z to a value larger than d, then z is replaced by its mirror image in the boundary, i.e., $d-(z-d)$. Similarly z is replaced by $-d+(-z-d)$ if z drops below $-d$. This method is the best way to keep z uniformly distributed in $[-d,d]$.

The initial condition consists in releasing all the particles at $t=0$ from a given initial radius r_0 at a height z_0 which is chosen uniformly in the interval $[-d,d]$. This represents an idealization of the experiment (another approach would be to modulate the random height z_0 according to the local flux of fluid as mentioned in Sec. II C).

The boundary condition at the injection radius is a little uncertain in the real laboratory experiment. We have chosen a reflecting boundary condition during the injection and an absorbing boundary condition during the withdrawal part of the echo experiment. Thus during the injection should a random displacement move r to be less than r_0, then r is replaced by $r_0+(r_0-r)$. Should a particle move to r less than r_0 during withdrawal, then it is said to have returned and is not moved again. Note that, as the random displacement is always larger than the convective displacement, about half of the particles are reflected on the first time step for small enough steps.

At regular time intervals in the computation, the mean and the variance of the radial positions are computed and recorded. As the particles return to the starting radius r_0, the mean and the variance of the return times are computed. Sometimes, there can be a long wait for the last particle to return. An early idea of only using the middle 80% of the particles, i.e., throwing away information about the first 10% to arrive and not waiting for the last 10% to arrive, was abandoned when it became clear that these extreme 20% were very influential on the values of the first and second moment.

The program solves a nondimensionalized problem. Distances are scaled on the channel half-width d, so that the channel depth coordinate satisfies $-1\leqslant z\leqslant 1$. Time is scaled with the time $\tau_m=d^2/D_m$ to diffuse across the channel half-width. Thus the nondimensional velocity involves the Péclet number based on the radius $\mathrm{Pe}_Q=Q/4\pi d D_m$ with

$$u(r,z)=\frac{3\,\mathrm{Pe}_Q}{2r}\,[1-z(t)^2]. \tag{26}$$

Typically 10^4 particles are required to give results accurate to nearly two significant figures. A few runs were made with 10^5 particles. A typical nondimensional time step was $\Delta t=10^{-4}$. This gives quite large random displacements of 0.024. For very short injection times and for very high Péclet numbers, shorter time steps like $\Delta t=10^{-5}$ were used. Typical Péclet numbers Pe_Q were of the order of 1000. Nearly all the calculations had the initial radius equal to the channel half-width ($r_0=1$ in nondimensional form).

For historical reasons the program time stepped the particles all along together instead of moving just one at a time until it had returned: It is indeed easier to compute the spatial distribution (which may be of interest) if all the particle positions are known simultaneously. This method is, however, slightly slower to execute (because of the indirect addressing on the vectors) and requires more RAM memory (in excess of the 64 K available under DOS Turbo Pascal). Computation times on a SUN4 were of the order of 10 min.

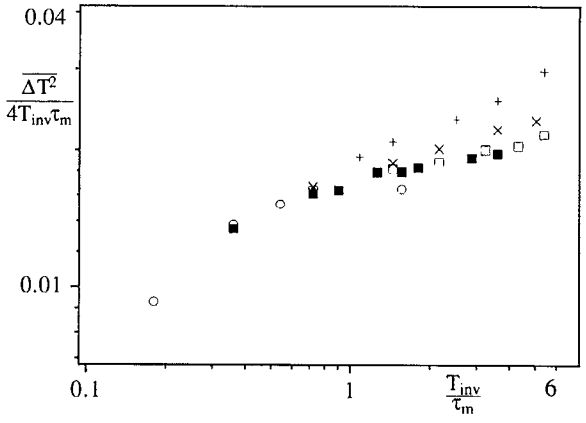

FIG. 3. Variation of the normalized second moment of the transit time distribution $\overline{\Delta t^2}/(4T_{\mathrm{inv}}\tau_m)$ as a function of the normalized inversion time T_{inv}/τ_m (in logarithmic scale) obtained from numerical simulations for several Péclet number values $\mathrm{Pe}_Q=Q/2\pi d=(+)530.5$, (×) 1061, (□) 2122, (■) 5305, and (○) 10 610.

B. Numerical results

The values of Pe_Q corresponding to the experimental flow rates that have been used are $\mathrm{Pe}_Q=530.5$, 1061, 2122, 5305, and 10 610. The inversion times at a given velocity were chosen so that the range of penetration depths remained the same as in the experiments.

We have analyzed the echo dispersion at short inversion times (Fig. 3) where $0.15\tau_m<T_{\mathrm{inv}}<5\tau_m$ and long inversion times (Fig. 4) with T_{inv} up to $10\tau_m$. In all cases we have studied the variations of the mean square devia-

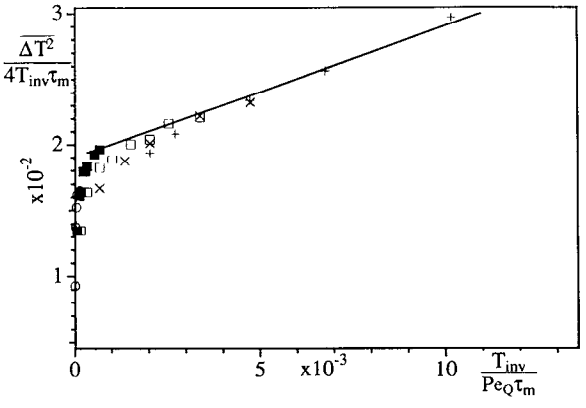

FIG. 4. Variation of the normalized second moment of the transit time distribution $\overline{\Delta t^2}/(4T_{\mathrm{inv}}\tau_m)$ as a function of the normalized inversion time $T_{\mathrm{inv}}/\mathrm{Pe}_Q\tau_m$ obtained from numerical simulations at various Péclet number values $\mathrm{Pe}_Q=(+)530.5$, (×) 1061, (□) 2122, (■) 5305, and (○) 10 610. The continuous straight line corresponds to the theoretical variation from Eq. (22).

tion $\overline{\Delta t^2}$ of the transit time normalized by the product of the inversion and the characteristic molecular diffusion times.

1. Short time behavior

Figure 3 shows the variation of the normalized second moment of the transit time distribution as a function of T_{inv}/τ_m. For inversion times between $0.3\tau_m$ and $1.5\tau_m$ we see that the variation of $\overline{\Delta t^2}/4T_{inv}\tau_m$ leads to a unique curve which is independent of the Péclet number (except for Pe=530.5). This result is in good agreement with Eq. (10).

Beyond $T_{inv} \geqslant 1.5\tau_m$, the curves spread out as the Péclet number decreases. This is associated with the longitudinal molecular diffusion through the term in $1/\mathrm{Pe}_Q$ [Eq. (22)] which becomes very important at low Péclet numbers (see $\mathrm{Pe}_Q = 530.5$).

On the other hand, we see that $\overline{\Delta t^2}/4T_{inv}\tau_m$ diminishes when T_{inv}/τ_m decreases. This corresponds to the variation of $\overline{\Delta t^2}/T_{inv}$ with $T_{inv}^{3/2}$ predicted by Eq. (17) when the transit time $2T_{inv}$ is too short to allow the tracer to diffuse across the full width of the channel.

2. Long time behavior

At the long injection times $T_{inv}/\mathrm{Pe}_Q\tau_m \gg 1$, longitudinal molecular diffusion becomes significant. In order to check Eq. (22), we have plotted in Fig. 4 the variation of $\overline{\Delta t^2}/(4T_{inv}\tau_m)$ as a function of $T_{inv}/(\mathrm{Pe}_Q\tau_m)$. We used the same Péclet numbers and extended the inversion times to $10\tau_m$. As the inversion time becomes greater than τ_m, we see that the normalized spread in the return times depends on $T_{inv}/(\mathrm{Pe}_Q\tau_m)$. We have superimposed on Fig. 4 the theoretical variation from Eq. (22). At short inversion times, the curves corresponding to different Péclet numbers are separate and they join the asymptotic theoretical curve at different values of $T_{inv}/(\mathrm{Pe}_Q\tau_m)$. This reflects the fact that, from Eq. (10), the variation of $\overline{\Delta t^2}/(4T_{inv}\tau_m)$ at short times is a universal function of T_{inv}/τ_m and not of $T_{inv}/(\mathrm{Pe}_Q\tau_m)$. When Pe_Q decreases, the values of $T_{inv}/(\mathrm{Pe}_Q\tau_m)$ at which the asymptotic linear variation of Eq. (22) is reached therefore become larger.

To summarize, the numerical simulations presented here allow us to determine quantitatively the boundaries between different dispersion regimes depending on values of T_{inv}/τ_m and $T_{inv}/(\mathrm{Pe}_Q\tau_m)$. The Taylor mechanism becomes established only when $T_{inv}/\tau_m > 1$. Longitudinal molecular diffusion is important if $T_{inv}/\tau_m > \mathrm{Pe}_Q/400$.

IV. EXPERIMENTAL MEASUREMENTS OF TRACER DISPERSION IN A RADIAL FLOW FIELD WITH A SMOOTH FRACTURE

A. Experimental setup

One model fracture, the "smooth fracture," consists of the gap between two square parallel 30 cm glass plates. In the other model, we replace the lower glass plate by a rough zinc one. The rough surface is made by a photoengraving process in which a computer generated pattern is etched with acid in a zinc plate. We used a mean spacing between plates $2d = 0.1$ cm in both cases.

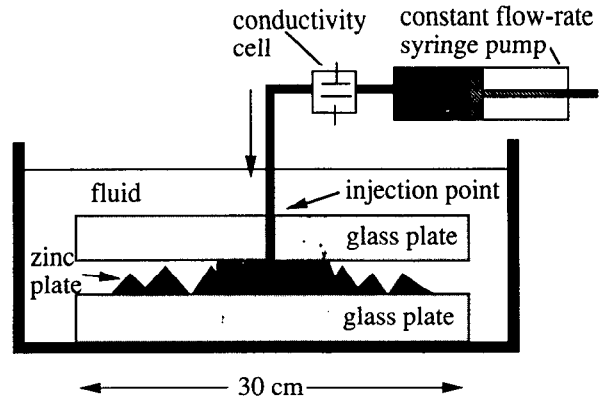

FIG. 5. Experimental setup.

The fluid is injected at the center of the model by a syringe pump with a constant flow rate Q and flows radially inside the cell (Fig. 5).

The assembly is immersed in a Plexiglas box partly filled with a sodium nitrate–water solution (1.5 g/l). This salt is used as the tracer. A low volume conductivity cell detector and a double syringe pump are connected to the injection point through a four-way valve. This allows one to inject or pump back either of two sodium nitrate solutions of different salt concentrations (1 or 1.5 g/l).

At the initial time ($t=0$), one induces an abrupt change in the concentration at the inlet by switching from the initial high salt concentration solution. The low concentration solution is then injected into the sample during a predefined time. The fluid flow is reversed and the variation in time of the tracer concentration $C(t)$ is determined from measurements of conductivity. We then calculate the tracer transit time distribution.

B. Quantitative analysis of the tracer dispersion

The experimental curves are fitted to solutions of the advection–diffusion equation (1) from which one can obtain the first and second moments $\bar{T}$ and $\overline{\Delta t^2}$ of the distribution of the tracer transit times. This determination is more precise than a direct computation of $\bar{T}$ and $\overline{\Delta t^2}$ from the rough data since it is less prone to the influence of noise and signal drifts, particularly at long times. Good fits of the experimental data by the Gaussian solutions were generally obtained. The experiments and data processing were performed for a large range of injection times and flow rates in both the rough and the smooth fractures.

We have first checked that the mean transit time $\bar{T}$ verified $\bar{T} = 2T_{inv}$: this relation might be broken by some trapping effects or by unwanted fluid leaks or flow-rate variations. Figure 6 shows the variation of $\bar{T}$ with T_{inv} for the smooth fracture (flow rate $Q = 3.2mL/mn$). We observe that the slope is very close to 2 as expected (a linear regression on the curve of Fig. 3 gives a slope value of 2.04). Also, the fitted straight line goes very nearly to zero,

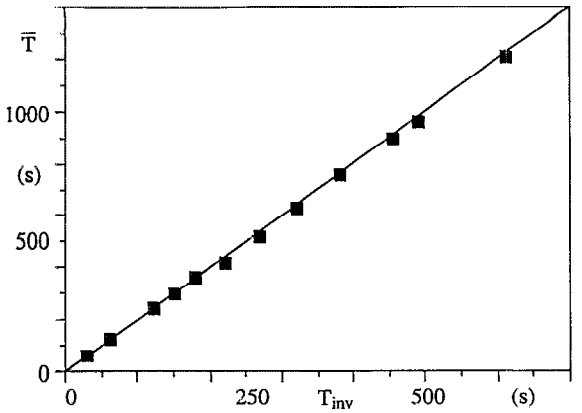

FIG. 6. Variation of the mean residence time as function of the injection time in a smooth fracture for a thickness $a=0.1$ cm and a flow rate $Q=3.2mL/mn$.

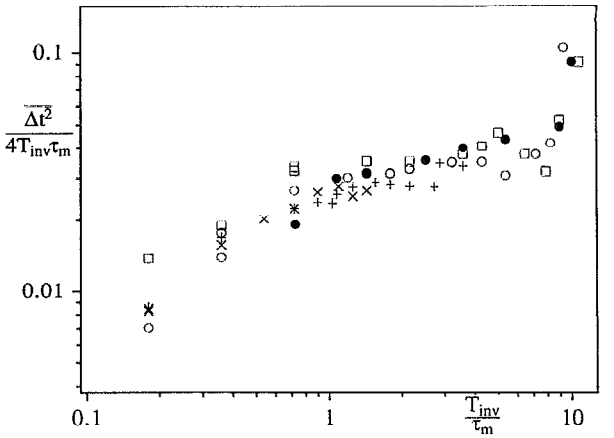

FIG. 8. Experimental variation of the mean square deviation of the transit time normalized as a function of the normalized injection time for a smooth fracture with a half-mean aperture $d=0.05$ cm (in logarithmic scale).

implying that there is a very small dead volume in the measurement system (which would introduce an additive term). We also compared the signal amplitude before and after the flow reversal which might also indicate irreversible trapping effects.

C. Tracer dispersion characteristics for fractures with smooth walls in radial flow

In the case of a fracture with smooth walls, we expect that $\overline{\Delta t^2}$ will have the same dependence on $\bar{T}$ and Q as discussed qualitatively and numerically earlier. In particular, while the Péclet number remains large, it should follow Eq. (10) and, more precisely, Eq. (9) for $t>\tau_m$.

Let us consider first the predictions of Eq. (9) for the variation of $\overline{\Delta t^2}$ with $\bar{T}$ at times long enough for the irreversible Taylor dispersion regime to be established. We have plotted in Fig. 7 the variation of $\overline{\Delta t^2}$ as a function of the mean transit time $\bar{T}$ $(=2T_{inv})$. Data points corresponding to two flow rates differing by a factor of 2 superimpose. We observe that both variations become linear for $T_{inv}\geqslant 100$ sec and that the slope of the curve does not

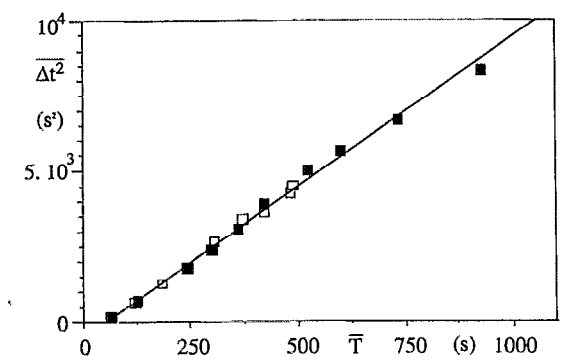

FIG. 7. Variation of the mean square deviation of the transit time $\overline{\Delta t^2}$ as a function of the mean transit time $\bar{T}$ for a smooth fracture with a half-mean aperture $d=0.05$ cm. Flow-rate values: (■) $Q=3.2mL/mn$ ($Pe_Q=5305$) and (□) $Q=6.4mL/mn$ ($Pe_Q=10\,610$).

depend on the flow rate, as predicted by Eq. (9). A linear regression gives a slope $d\overline{\Delta t^2}/d\bar{T}=10$ sec. Using Eq. (9) and the value $D_m=1.5\times10^{-5}$ cm^2 sec^{-1} for the molecular diffusion coefficient we obtain the effective value $d_{eff}\simeq0.056$ cm for the half-interval d between the plates. This is in reasonable agreement with the thickness $2d=(0.1\pm0.01)$ cm measured directly.

In order to determine whether Eq. (10) is valid at short times, we have plotted in Fig. 8 the variation of $\overline{\Delta t^2}/(4T_{inv}\tau_m)$ as a function of T_{inv}/τ_m. The characteristic diffusion time is $\tau_m=d^2/D_m\simeq167$ sec (for $d=0.05$ mm). Figure 8 shows that, for $T_{inv}/\tau_m<3$, all experimental points are, within experimental error, located on the same curve independent of the flow rate (in the range $500<Pe_Q<10\,000$). Note, however, that, as expected, data points for low Péclet numbers are, on the average, slightly above those corresponding to higher values of Pe_Q. These results prove that the ratio $\overline{\Delta t^2}/(4T_{inv}\tau_m)$ is almost independent of the Péclet number, in good agreement with the hypothesis that molecular diffusion perpendicular to the plates is the dominant mechanism to induce irreversibility.

For $T_{inv}/\tau_m<1$, the ratio $\overline{\Delta t^2}/(4T_{inv}\tau_m)$ decreases as the injection time is reduced as predicted from Eq. (18). Figure 8 shows that $\overline{\Delta t^2}/(4T_{inv}\tau_m)$ follows a "universal" law as predicted by Eq. (9) at short injection times where the Taylor regime is not yet established.

For $1<T_{inv}/\tau_m<3$ and at the higher Péclet numbers $\overline{\Delta t^2}/(4T_{inv}\tau_m)$ is about constant and equal to 0.025, i.e., 30% larger than the theoretical value 2/105. This ratio $\overline{\Delta t^2}/(4T_{inv}\tau_m)$ decreases close to the theoretical value if one uses the value $d=0.056$ found above for the thickness (giving $\tau_m\cong210$ sec).

For $3<T_{inv}/\tau_m<7$, we observe a marked increase of the ratio $\overline{\Delta t^2}/(4T_{inv}\tau_m)$, particularly at the lowest flow rate corresponding to $Pe_Q=530.5$ ($Q=0.3mL/mn$). This variation is in qualitative agreement with the numerical simulations shown in Fig. 3. The increase seems to reflect the

influence of the additional contribution $T_{inv}/(Pe_Q\tau_m)$ to $\overline{\Delta t^2}/(4T_{inv}\tau_m)$ which appears in Eq. (22) due to longitudinal molecular diffusion. This confirms that the "universal" behavior for pure Taylor dispersion disappears at low Péclet numbers and long times.

In conclusion, our experimental results in the smooth radial model confirm that the ratio $\overline{\Delta t^2}/(4T_{inv}\tau_m)$ depends only on the ratio T_{inv}/τ_m as long as the local velocity is high enough for longitudinal molecular diffusion to be neglected. In this case, the dependence on T_{inv}/τ_m is the same as for a constant velocity parallel flow. At low velocities and long times, the effect of molecular diffusion becomes significant because velocity decreases at large distances. This leads to an increase of $\overline{\Delta t^2}/(4T_{inv}\tau_m)$ equal to $T_{inv}/Pe_Q\tau_m$.

V. EXPERIMENTAL MEASUREMENTS OF TRACER DISPERSION IN A RADIAL FLOW IN A ROUGH FRACTURE

A. Effect of roughness on Taylor dispersion between parallel planes

Let us now consider a fracture with rough walls. The roughness introduces a spatial disorder in the velocity field in the directions parallel to the fracture surface. In 3-D porous media, it has been shown that such disorder contributes to the dispersion coefficient a term proportional to the flow velocity.[6,17] This dispersion mechanism due to velocity variations from one pore channel to another is called geometrical dispersion. It is dominant in 3-D porous media at medium and high Péclet number, $Pe > 10$. Then, $D_{\parallel}$ varies linearly with the mean velocity

$$D_{\parallel} = l_D U, \tag{27}$$

where l_D is called dispersion length or dispersivity. For homogeneous packings of nonporous grains, l_D is the order of the grain size and is constant with the velocity. For heterogeneous materials such as natural rocks or sintered samples, l_D can be much larger than the grain size. In geometrical dispersion, tracer particles make a random walk controlled by the spatial disorder of the pore space. At the same time, they are carried through the medium at the average flow velocity. The dispersion length l_D is the length of the steps of the random walk. The dispersion $D_{\parallel}$ is the integral of the correlation of the velocity fluctuations along the path of a tracer particle

$$D_{\parallel} = \left\langle \int_0^t [u_{\parallel}(0) - U][u_{\parallel}(t) - U]dt \right\rangle. \tag{28}$$

In Eq. (28), $u_{\parallel}$ represent the velocity component of a tracer particle along the mean velocity **U**. The integral is taken along the path of the particle and the angle brackets represent an ensemble average over all possible trajectories.[18,19]

In planar 2-D fractures with rough walls, Taylor and geometric dispersion processes are active simultaneously, particularly at high flow velocities[20,21] whereas in 3-D materials, only geometrical dispersion is significant at high velocities. This key feature is due to the fact that in 2-D systems tracer particles can only move away from low-velocity zones close to the upper and lower solid surfaces through molecular diffusion. Even with rough walls, the flow lines follow the contour of the continuous solid boundaries. Therefore, the effect of the parabolic velocity profile across the aperture of the fracture will be felt by the tracer particles until they have explored the interval between plates through molecular diffusion.

The geometrical and Taylor dispersion effects thus add up since the influence of the geometrical disorder will not be decreased by the transverse molecular diffusion. In the case of a constant velocity flow and at long times compared to τ_m, the dispersion coefficient should be given by

$$D_{\parallel} = \frac{a_{eff}^2 U^2}{210 D_m} + l_g U + D_m, \tag{29}$$

where $a_{eff} = 2d_{eff}$ is an effective thickness taking into account the effect of the roughness: for smooth plates, a_{eff} will be equal to the actual spacing $2d$.

For comparison, in 3-D porous media, tracer particles that are close to the solid walls of an individual grain will generally leave the grain close to a stagnation point and will then find themselves in a high-velocity zone in the middle of a flow channel. Taylor diffusion will only be significant at velocities (i.e., at Péclet numbers) low enough so that one can diffuse significantly across the flow channels during the transit time along *one* individual channel (with a length of the order of the grain size).

In the case of the radial flow geometry and if $T_{inv} \gg \tau_m$, Eq. (29) will retain locally the same variation with the local flow velocity $U[r(t)] = \frac{1}{2}\sqrt{(Q/2\pi d)}\, t^{-1/2}$ [after replacing $r(t)$ by its value from Eq. (7b)].

The mean square deviation of the tracer transit time can be estimated by integrating Eq. (20b) with D from expression (29). Thus we have

$$\frac{\overline{\Delta t^2}}{4T_{inv}} = \frac{2d^2}{105 D_m} + \frac{2}{3}\sqrt{8\pi}\, l_g \sqrt{\frac{dT_{inv}}{Q}} + 8\pi D_m \left(\frac{dT_{inv}}{Q}\right). \tag{30}$$

The first term comes from Taylor dispersion, the second term from geometrical dispersion, and the last term from molecular diffusion.

B. Experimental results

The rough model fracture consists of the same experimental setup as in Sec. IV with the lower glass plate replaced by a rough surface. We used a mean spacing between plates of $a = 2d = 0.1$ cm and we have used the same range of injection flow rates Q as in the smooth fracture (from $0.3mL/mn$ to $6mL/mn$). For each constant flow rate we performed several echo dispersion experiments at different injection times (for instance, at $Q = 0.3mL/mn$, $60 \text{ sec} \leqslant T_{inv} \leqslant 2700 \text{ sec}$).

In order to estimate the magnitude of the geometrical dispersion included in Eq. (30), we have plotted in Fig. 9 the ratio $\overline{\Delta t^2}/4T_{inv}$ as a function of $\sqrt{dT_{inv}/Q}$. We observe that, provided $\bar{T} > \tau_m$, all the experimental data follow the same linear variation independent of the injection flow rate.

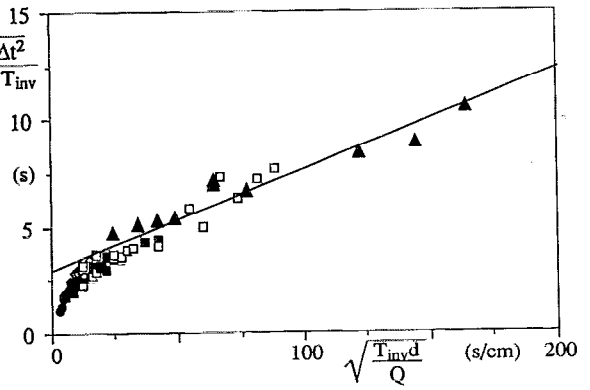

FIG. 9. Variation of $\overline{\Delta t^2}/4T_{inv}$ as a function of $\sqrt{dT_{inv}/Q}$ for a fracture with a rough wall. Mean spacing between plates is taken 0.1 cm (d=0.05 cm). The corresponding injections flow rates are (●) $6mL/mn$, (◇) $3.2mL/mn$, (■) $1.2mL/mn$, (□) $0.6mL/mn$, and (▲) $0.3mL/mn$. The straight line corresponds to a linear regression taken over data points satisfying $T_{inv} > \tau_m$.

The small time variation of $\overline{\Delta t^2}/4T_{inv}$ depends only on the ratio T_{inv}/τ_m so that this part of the data does not superimpose on Fig. 9. The universal linear variation is reached at larger and larger values of dT_{inv}/Q as Q decreases. A linear regression using the mean width $2d$=0.1 cm measured by mass conservation gives

$$\frac{\overline{\Delta t^2}}{4T_{inv}}\,(s) = 2.99 + 4.64 \times 10^{-2}\sqrt{\frac{dT_{inv}}{Q}}. \tag{31}$$

Identifying this expression with Eq. (30) we obtain the transverse molecular diffusion time through: $2\tau_m/105 = 2.99$ sec whence $\tau_m = 157$ sec. From this value, we compute an effective half-mean aperture for molecular diffusion $d_{eff} = 0.048$ cm, in good agreement with that measured by mass conservation.

The second coefficient $\frac{2}{3}\sqrt{8\pi l_g} = 4.64 \times 10^{-2}$ cm, allows us to estimate the value of the characteristic dispersion length, $l_g \cong 0.01$ cm. This is to be compared to the typical size of the roughness elements of the zinc plates which is of the order of 0.1 cm. In some sense, the roughened plate is only 10% efficient at producing geometric dispersion: A major objective of future experiments will be to characterize quantitatively the rough surface geometry.

VI. CONCLUSION

In the present paper we have demonstrated experimentally and through numerical simulation that echo tracer dispersion allows one to obtain quantitative information about the local structure of plane fractures with a radial flow field, e.g., the thickness and the roughness.

In fractures with smooth walls, the mean square deviation of the transit time $\overline{\Delta t^2}$ has the same variation with the mean residence time $\bar{T} = 2T_{inv}$ in radial and parallel flow fields (T_{inv} is the time after which the flow direction is reversed). This occurs provided the flow is large enough for longitudinal molecular diffusion to be negligible throughout the flow [local Péclet number $U(r)d/D_m \gg 1$]. In this case, the ratio $\overline{\Delta t^2}/(T_{inv}\tau_m)$ reaches a constant value at long times $T_{inv} > \tau_m$ (τ_m is the characteristic diffusion time over the half-interval d between plates). At short injection times $T_{inv} < \tau_m$, the ratio $\overline{\Delta t^2}/(T_{inv}\tau_m)$ is a function of T_{inv}/τ_m independent of geometry and the velocity (if it is large enough); the echo dispersion is less than the asymptotic limit because Taylor dispersion is not fully established with T_{inv} too small to allow the tracer concentration to homogenize across the flow section. In this short time range, $\overline{\Delta t^2}/(T_{inv}\tau_m)$ varies as $(T_{inv}/\tau_m)^{3/2}$ or $(T_{inv}/\tau_m)^2 \log(T_{inv})$ depending on the type of tracer injection (constant concentration or constant flux).

At low flow rates and long transit times, it is no longer possible to neglect the longitudinal molecular diffusion which contributes to $\overline{\Delta t^2}/(T_{inv}\tau_m)$ an additional term: $4T_{inv}/(\mathrm{Pe}_Q\tau_m)$, where $\mathrm{Pe}_Q = Q/(2\pi dD_m)$ is the Péclet number using the radial distance as the characteristic length scale (Q is the injected volume flow rate). This contribution proportional to the injection time is associated with the decrease of the flow velocity with the distance from the injection point and will not be observed in parallel constant velocity flows.

When one of the fracture walls is rough, the disorder associated with the roughness may induce some geometrical dispersion. The corresponding additional dispersion term is proportional to $\sqrt{dT_{inv}/Q}$ and appears clearly in the experimental results.

Several aspects need, however, to be clarified for a good understanding of the process. A first question is the quantitative relation between the geometrical dispersion and the structure of the roughness elements. Another is the influence of defects in the symmetry of the flow field, because actual flow fields will neither be radial nor parallel. One interesting feature of echo tracer dispersion is the fact that macroscopic differences in the length and the velocity of different flow paths have a reduced influence, because particles injected along one path retrace that path during the withdrawal phase. However, transverse molecular diffusion or geometrical dispersion may allow the particles to move from one macroscopic flow path to another.

ACKNOWLEDGMENTS

One of us (I. Ippolito) has been partly supported through funding by EFDS Dowell–Schlumberger and Schlumberger Cambridge Research.

[1] L. Moreno, Y. W. Tsang, C. F. Tsang, F. V. Hale, and I. Neretnieks, "Flow and tracer transport in a single fracture: A stochastic model and its relation to some field observations," Water Resour. Res. **24**, 2033 (1988).

[2] L. De Arcangelis, J. Koplik, S. Redner, and D. Wilkinson, "Hydrodynamic dispersion in network models of porous media," Phys. Rev. Lett. **57**, 996 (1986).

[3] E. Charlaix, E. Guyon, and S. Roux, "Permeability of an array of fractures with randomly varying apertures," Transport Porous Media **2**, 31 (1987).

[4] S. Roux, J. Schmittbuhl, J. P. Vilotte, and A. Hansen, "Some physical properties of self-affine rough surfaces" Europhys. Lett. (to be published).

[5] F. A. L. Dullien, *Porous Media, Fluid Transport and Pore Structure*, 2nd ed. (Academic, New York, 1992).

[6]J. Bear, *Dynamics of Fluids in Porous Media* (Elsevier, New York, 1972).
[7]R. N. Horne and F. Rodriguez, "Dispersion in tracer flow in fractured geothermal systems," Geophys. Res. Lett. **10**, 289 (1983).
[8]J. P. Hulin and T. J. Plona, "Echo tracer dispersion in porous media," Phys. Fluids A **1**, 1341 (1989).
[9]C. Leroy, J. P. Hulin, and R. Lenormand, "Tracer dispersion in stratified porous media: Influence of transverse dispersion and gravity," J. Contam. Hydrol. **11**, 51 (1992).
[10]G. I. Taylor, "Dispersion of soluble matter in solvent flowing slowly through a tube," Proc. R. Soc. London Ser. A **219**, 186 (1953).
[11]R. Aris, "On the dispersion of a solute in a fluid flowing through a tube," Proc. R. Soc. London Ser. A **235**, 67 (1956).
[12]J. C. Bacri, J. P. Bouchaud, A. Georges, E. Guyon, J. P. Hulin, N. Rakotomalala, and D. Salin, "Non-Gaussian tracer dispersion in porous media," *Proceedings of the 4th EPS Conference on the Hydrodynamics of Dispersed Media*, Arcachon, France, edited by E. Guyon, F. Carmona, A. M. Cazabat, and J. P. Hulin (North-Holland, Amsterdam, 1990), pp. 249–269.
[13]J. F. Brady, "Dispersion in heterogeneous media," in Ref. 12, pp. 271–285.
[14]P. G. de Gennes, "Hydrodynamic dispersion in unsaturated porous media," J. Fluid Mech. **136**, 189 (1983).
[15]J. Koplik, "Hydrodynamic dispersion in random networks," in *Disorder and Mixing*, edited by E. Guyon, J. P. Nadal, and Y. Pomeau (Kluwer Academic, Dordrecht, The Netherlands, 1988), Chap. 7, pp. 123–137.
[16]G. K. Batchelor, in *Introduction to Fluid Dynamics* (Cambridge University Press, Cambridge, 1970), Chap. 4.
[17]P. G. Saffman, "A theory of dispersion in porous medium," J. Fluid Mech., Part 3, **6**, 341 (1959).
[18]D. L. Koch and J. F. Brady, "Dispersion in fixed beds," J. Fluid Mech. **154**, 399 (1985).
[19]J. F. Brady and D. L. Koch, "Dispersion in porous media," in Ref. 15, Chap. 6, pp. 107–122.
[20]I. Ippolito, G. Daccord, P. Kurowski, and J. P. Hulin, "Tracer transport properties in heterogeneous 2-D structures for parallel and radial flow geometries," *Proceedings of the Fractured and Jointed Rock Masses Conference*, Lake Tahoe, CA, 3–5 June 1992, edited by L. W. Myer (Balkema, to be published).
[21]E. Charlaix, J. P. Hulin, C. Zarcone, and C. Leroy, "Experimental study of tracer dispersion in flow through two-dimensional networks of etched capillaries," J. Phys. D: Appl. Phys. **21**, 1727 (1988).